ECS Journal of Solid State
Science and Technology

Prussian Blue Analogous $Na_2Ni_{0.33}Co_{0.33}[Fe(CN)_6]$ Nanoparticles as Cathode Material for Non-Aqueous Na-Ion Batteries

ECS Journal of Solid State Science and Technology, 2021 **10** 061012
2162-8777/2021/10(6)/061012/5/$40.00 © 2021 The Electrochemical Society ("ECS"). Published on behalf of ECS by IOP Publishing Limited

Prussian Blue Analogous $Na_2Ni_{0.33}Co_{0.33}[Fe(CN)_6]$ Nanoparticles as Cathode Material for Non-Aqueous Na-Ion Batteries

Akhil Shettigar,[1,=] Brindha Moorthy,[2,=] Vivek Paulraj,[1] Do Kyung Kim,[2,z] and K. Kamala Bharathi[1,3,z]

[1]*Department of Physics and Nanotechnology, SRM Institute of Science and Technology, Kattankulathur, Chennai– 603203, India*
[2]*Department of Materials Science and Engineering, Korea Advanced Institute of Science and Technology (KAIST), Daejeon, 34141, Republic of Korea*
[3]*Nanotechnology Research Center (NRC), SRM Institute of Science and Technology, Kattankulathur, Chennai–603203, India*

We report on the electrochemical properties of 20 nm $Na_2Ni_{0.33}Co_{0.33}[Fe(CN)_6]$ nanoparticles. $Na_2Ni_{0.33}Co_{0.33}[Fe(CN)_6]$ nanoparticles overcome the poor electronic conductivity and deliver an initial charge capacity of 77 mAh g^{-1} at 0.1C rate and and 55 mAh g^{-1} after 320 cycles at 1C rate. At high current rate of 5C, they deliver 35 mAh g^{-1} and exhibit almost 100% columbic efficiency. The single redox sodium ion chemistry with 3 V makes the material suitable for non-aqueous sodium ion batteries. The redox couple Fe^{3+}/Fe^{2+} is seen to be electrochemically active during the charge/discharge process, which is confirmed by ex situ X-ray photon spectroscopy.
 [DOI: 10.1149/2162-8777/ac0a42]

Manuscript submitted April 27, 2021; revised manuscript received June 2, 2021. Published June 22, 2021. *This paper is part of the JSS Focus Issue on Selected Papers from the International Conference on Nanoscience and Nanotechnology 2021 (ICONN-2021).*

There are numerous ways to generate renewable energy in this modern world while the energy storage has no other better option than batteries. The eco-friendly renewable energy is more effective only if it has cost effective storage solution.[1] Lithium-ion batteries (LIBs) are successful in commercialization and reached hand held gadgets. LIBs are not feasible for static electric grid storage because of its low abundance; moreover weight does not matter for such applications.[2] The sodium ion batteries (SIBs) are the possible solution for the quest of cheaper and large scale energy storage that could rescue us from the too much dependence on LIBs.[3–5] Static grid energy storage demands cheaper than lighter material, which makes SIBs suitable. There are large numbers of cathode materials explored so far, including polyanions and pyrophosphates,[6–8] Oxides,[9–11] organic materials and Prussian blue analogues (PBA).[12–14] Though Prussian blue exhibits an open three-dimensional channel for Na + ion movement with a capacity of 95 mAh g^{-1} and 100% columbic efficiency, it suffers poor cycling that restricts its commercialization.[15]

SIBs need to overcome lots of obstacles in improving its chemistry. The sodium ion has larger ionic radius Na^+ (1.02 Å) which is responsible for slow diffusion, needs materials with large ionic channels. The electronic conductivity of the PBAs is low, which leads to sluggish Na + diffusion affecting rate capability.[16] Compared to all other cathode materials, PBAs has lot of advantages due to its stable crystalline structure that favors intercalation/deintercalation, high theoretical capacity and simple synthesizing methods. Open three dimensional networks with the (C-N) anions in the Prussian blue analogous have enough space to support fast ionic diffusion.[17–19] By shortening the diffusion path of Na^+ ions, the rate capability of the material can be improved which can be accomplished by synthesizing the material with nano dimension.[20] The substitution of cobalt is known for stabilizing structure and enhancing stability of Li^+ ion cathodes.[21,22] Also substituting Fe with other electrochemically active transition metals can alter the electrochemical redox potential, without disturbing the crystal structure. Co and Ni substitutions are known for increasing the PBAs redox voltage.[23–25] It has been reported that the substitution of nickel also can stabilize the PBAs structure.[26] Single Na^+ insertion materials usually have less strain compared to double Na^+ insertion materials with single redox peak, which favors reliable and durable source of energy with high stability and longevity. Most of the double Na^+ insertion materials possess double redox, which would make way for unstable cell voltage. On the other hand, single Na^+ insertion materials have single redox behavior.[27]

In the present case, we have synthesized PBAs nanoparticles ($Na_2Ni_{0.33}Co_{0.33}[Fe(CN)_6]$) by simple co-precipitation method with single Na^+ insertion chemistry. Co and Ni (in 1:1 ratio) are partially substituted at Fe site in the Prussian blue structure and the electrochemical properties are explored. The electrochemical properties of $Na_2Ni_{0.33}Co_{0.33}[Fe(CN)_6]$ nanoparticles is explored at different charge/discharge rates and discussed in this manuscript. In addition to that, changes in the oxidation states of all the elements present in $Na_2Ni_{0.33}Co_{0.33}[Fe(CN)_6]$ is explored via the ex situ X-ray photoelectron spectroscopy (XPS). The obtained results are discussed and presented in the manuscript.

Experimental

$Na_2Ni_{0.33}Co_{0.33}[Fe(CN)_6]$ nanoparticles were synthesized at room temperature by simple co-precipitation method. All the starting materials were purchased from Sigma Aldrich. Stoichiometric $NiNO_3.6H_2O$ (0.033 M) and $Co(NO_3)_2.6H_2O$ (0.033 M) powders were dissolved in 50 ml de-ionized (DI) water under strong magnetic stirring (Solution 1). Simultaneously, $Na_4Fe(CN)_6$ (0.05 M) powder was dissolved in 50 ml DI water along with 7 times the weight in grams of NaCl and kept under strong magnetic stirring (Solution 2). Subsequently, Solution 1 was added drop wise through a burette into Solution 2 under vigorous stirring. The suspension was aged for 24 h. The resulting precipitate was washed with DI water and ethanol and dried in oven for 80 °C for 12 h.

Material Characterization

The structural properties of $Na_2Ni_{0.33}Co_{0.33}[Fe(CN)_6]$ nanoparticles were characterized by employing X-ray diffractometer (XRD, Rigaku, D/MAX-IIIC X-ray diffractometer, Tokyo, Japan). Morphology of the samples was characterized by using high resolution transmission electron microscope (HR-TEM, JEOL, Japan). Oxidation states of the elements were analyzed using X-ray Photon Spectrometry (Physical Electronics, JAPAN). All the electrochemical studies were carried out using Wonatech potentiostat. The electrochemical studies were conducted with the fabrication of CR2032 coin cells. Powder slurry was prepared by mixing $Na_2Ni_{0.33}Co_{0.33}[Fe(CN)_6]$ with ketjen black and PVDF binder using NMP solvent under the ratio of 70:20:10 and the

[=]These authors contributed equally to the work.
[z]E-mail: dkkim@kaist.ac.kr; kamalabk@srmist.edu.in

slurry was coated on copper foil with a mass loading of ~1.5–2 mg cm^{-2}. The coated electrode was dried in a vacuum oven for 12 h. The material coated foil was cut into 12 mm diameter electrode using the crimping tool. The electrochemical studies were preceded in a half cell configuration. Na metal foil was cut with 12 mm diameter and used as an anode for the cell. 1 M $NaClO_4$ solution in $CH_3C_2H_3O_2CO$ (propylene carbonate) with 2% of Fluoroethylene carbonate was prepared and used as working electrolyte. Glass borosilicate fibre was used as separator. The coin cell with the coated electrode was assembled inside Argon filled glove box. Cycled cells were opened and dried inside the glove box and packed well to carry out the ex situ XRD and XPS measurements. Without any delay, samples were loaded in an inert XPS chamber for the ex situ measurements.

Results and Discussion

XRD pattern of as synthesized $Na_2Ni_{0.33}Co_{0.33}[Fe(CN)_6]$ sample is shown in the Fig. 1. The XRD pattern indicates the formation of $Na_2Ni_{0.33}Co_{0.33}[Fe(CN)_6]$ (JCPDS No. 52–1907) in face centered cubic (FCC) structure of Prussian blue analogues with the space group of Fm-3m. Lattice parameter values are calculated to be $a = b = c = 10.251$ Å, agrees well with the reported value. The calculated X-ray density value for the material is 1.617 gm cm^{-3}. In the FCC lattice, Co and Ni atoms are coordinated by six nitrogen atoms and six carbon atoms are coordinated with Fe atom. The arrangement of Co and Ni atoms in octahedral site with six nitrogen atoms coupled with the FeC_6 octahedra by cyanide group makes way to formation of 3D network that facilitates the sodium ion diffusion.[28]

The morphological study of the $Na_2Ni_{0.33}Co_{0.33}[Fe(CN)_6]$ powders were carried out using TEM and the images are shown in Fig. 2. TEM results depicts that the particles are agglomerated and spherical in shape with average particle size of ~ 20 nm (Figs. 2a and 2b). The elements present in the sample are confirmed with energy dispersive X-ray analysis, which displays the presence of C, N, Na, Ni, Co and Fe (Fig. 2c). No other element is seen to be present in the sample, indicating the high pure nature of the $Na_2Ni_{0.33}Co_{0.33}[Fe(CN)_6]$.

Valence states of the individual elements in $Na_2Ni_{0.33}Co_{0.33}[Fe(CN)_6]$ are investigated with X-ray Photon Spectroscopy and are presented in Fig. 3. The survey spectrum (Fig. 3a) indicates the presence of C, N, Co, Ni and Fe in the sample. The XPS spectrum was deconvoluted using Gaussian function. peak corresponding to carbon (Fig. 3b) is deconvoluted into three peaks centered at 288.65, 285.18 and 284.77 eV. The peak at 288.65 eV, 285.18 eV and 284.77 eV is attributed to C=O bonds, C–N bonds and C–C (sp^3) bonds respectively.[29–35] Figure 3c shows the XPS peak of Nitrogen, which is deconvoluted into three peaks centered at 402.24, 398.46 and 397.86 eV. The peak at 402.24 eV, 398.86 eV and 397.86 eV is due to the C≡N bonds, N–C (sp^3) bonds and the N–C (sp2) bonds respectively.[35] The Ni 2*p* peaks centered at 856.32 eV and 858.06 eV (Fig. 3d) are corresponding to Ni $2p_{3/2}$ Ni^{3+} and Ni^{2+} states and the additional peaks at 874.07 eV and 877.49 eV corresponds to Ni $2p_{1/3}$ Ni^{3+} and Ni^{2+} oxidation states. In addition to that, satellite peak is also observed at 863.16 eV.[29,30] The XPS peaks of Co 2*p* is shown in Fig. 3e which are centered at 781.81 eV and 784.90 eV, arising from Co $2p_{3/2}$ Co^{3+} and Co^{2+} states respectively. The peaks centered at 797.59 eV and 802.45 eV arises due to the Co $2p_{1/3}$ Co^{3+} and Co^{2+}states. A satellite peak is also observed at 789.21 eV.[31] The peaks corresponding to Fe 2*p* is shown in Fig. 3f. Peaks centered at 708.53 eV and 709.89 eV arises from Fe $2p_{3/2}$ Fe^{3+} and Fe^{2+} states respectively. Peaks at 721.41 eV and 723.31 eV corresponds to Fe $2p_{1/3}$ Fe^{3+} and Fe^{2+} states.[32,33] In addition to that, two satellite peaks are seen to appear at 716.52 and 712.84 eV. XPS studies clearly indicate that the Ni, Co and Fe elements exhibit in mixed oxidation states of +2 and +3 in the pristine sample.

The cyclic voltammetry (CV) measurement is carried out between the potential ranges of 2.5–4.2 V with different current sweep rates 150, 250 and 500 mVs^{-1} current sweep rate and the

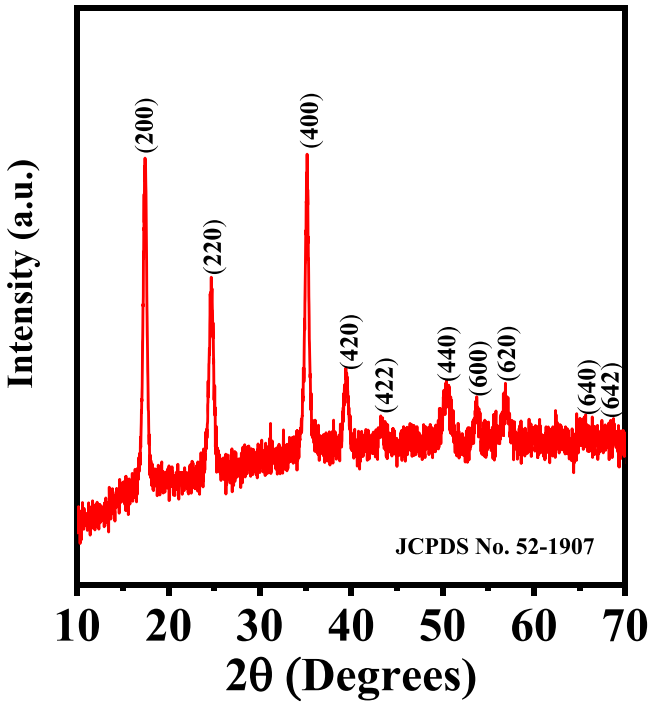

Figure 1. XRD pattern of $Na_2Ni_{0.33}Co_{0.33}[Fe(CN)_6]$ nanoparticles.

results for the first five cycles are presented in Fig. 4a. The CV curves shows oxidation peaks from 3.6 to 3.8 V and reduction peaks at 2.7 to 3 V with increase in scan rates. The redox peaks between 2.7 V to 3.8 suggests that the $[Fe(CN)_6]^{4-/3-}$ couple takes place during the redox reaction. While charging, the sodium ion from the cathode material moves from the crystal lattice and deposit on the sodium foil and the reverse happens on discharging.[36,37] The sodium ion removal from the crystal lattice alter the Fe(II) oxidation state to Fe(III) state and the reverse occurs on discharging. The high working potential range (2.7 to 3.8 V) suggests that the $Na_2Ni_{0.33}Co_{0.33}[Fe(CN)_6]$ nanomaterials can be used as a viable cathode material for Na ion batteries. The charge and discharge characteristics of $Na_2Ni_{0.33}Co_{0.33}[Fe(CN)_6]$ nanomaterials is investigated between the voltage window of 2.5–4.2 V at different charge (C)-rates. Figure 4b shows the charge and discharge profile of $Na_2Ni_{0.33}Co_{0.33}[Fe(CN)_6]$ nanomaterials at different C rates of 0.1, 0.2, 0.5, 1, 2 and 5C. $Na_2Ni_{0.33}Co_{0.33}[Fe(CN)_6]$ nanomaterial exhibit the charging capacity of 77 mAh g^{-1} and discharging capacity of 64 mAh g^{-1} at 0.1C rate. The consecutive charge discharge profiles show the excellent performance at high C rates. The rate capability of $Na_2Ni_{0.33}Co_{0.33}[Fe(CN)_6]$ nanomaterial is analyzed at different charge/discharge rates such as 0.1, 0.2, 0.5, 1, 2 and 5C that are shown in Fig. 4c along with the Coulombic efficiency. The rate of $Na_2Ni_{0.33}Co_{0.33}[Fe(CN)_6]$ nanomaterial indicates the capability for high current applications. The Fig. 4**d** shows the charge capacity and the Coulombic efficiency of $Na_2Ni_{0.33}Co_{0.33}[Fe(CN)_6]$ nanomaterials for 320 cycles at 1C rate. The initial charge capacity is 62 mAh g^{-1} and after 320th cycle is seen to be 55 mAh g^{-1}. Coulombic efficiency of 100% throughout the charge/discharge cycle at different C rates indicates the good stability of the material. Table I depicts comparison of electrochemical performance of PBA material with the similar materials reported in the literature.

The changes in oxidation state of the elements present in the $Na_2Ni_{0.33}Co_{0.33}[Fe(CN)_6]$ nanomaterial during the electrochemical process is analyzed by ex situ XPS analysis (Fig. 5). XPS spectra were recorded on the cycled electrodes after 1st charge (Figs. 5a to 5d) and 2nd discharge (Figs. 5e to 5h) and are shown in Fig. 5. The survey spectrum after 1st charge and 2nd discharge suggests the elements Na, Ni, Co, Fe, C and N are present in the sample. The Figs. 5a and 5e were plotted between binding energy and counts per

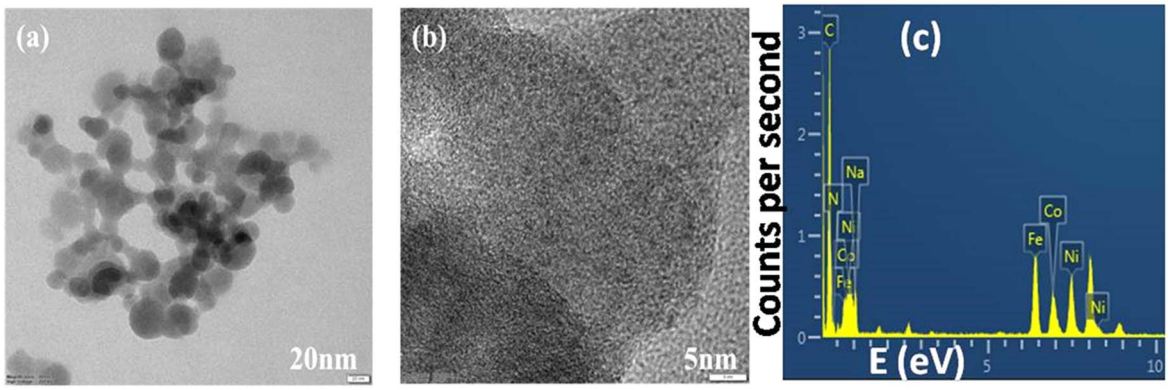

Figure 2. TEM images of $Na_2Ni_{0.33}Co_{0.33}[Fe(CN)_6]$ nanoparticles (a) and (b), indicating the spherical particles witn 20 nm size. Energy dispersive X-ray spectra of $Na_2Ni_{0.33}Co_{0.33}[Fe(CN)_6]$ nanoparticles (c).

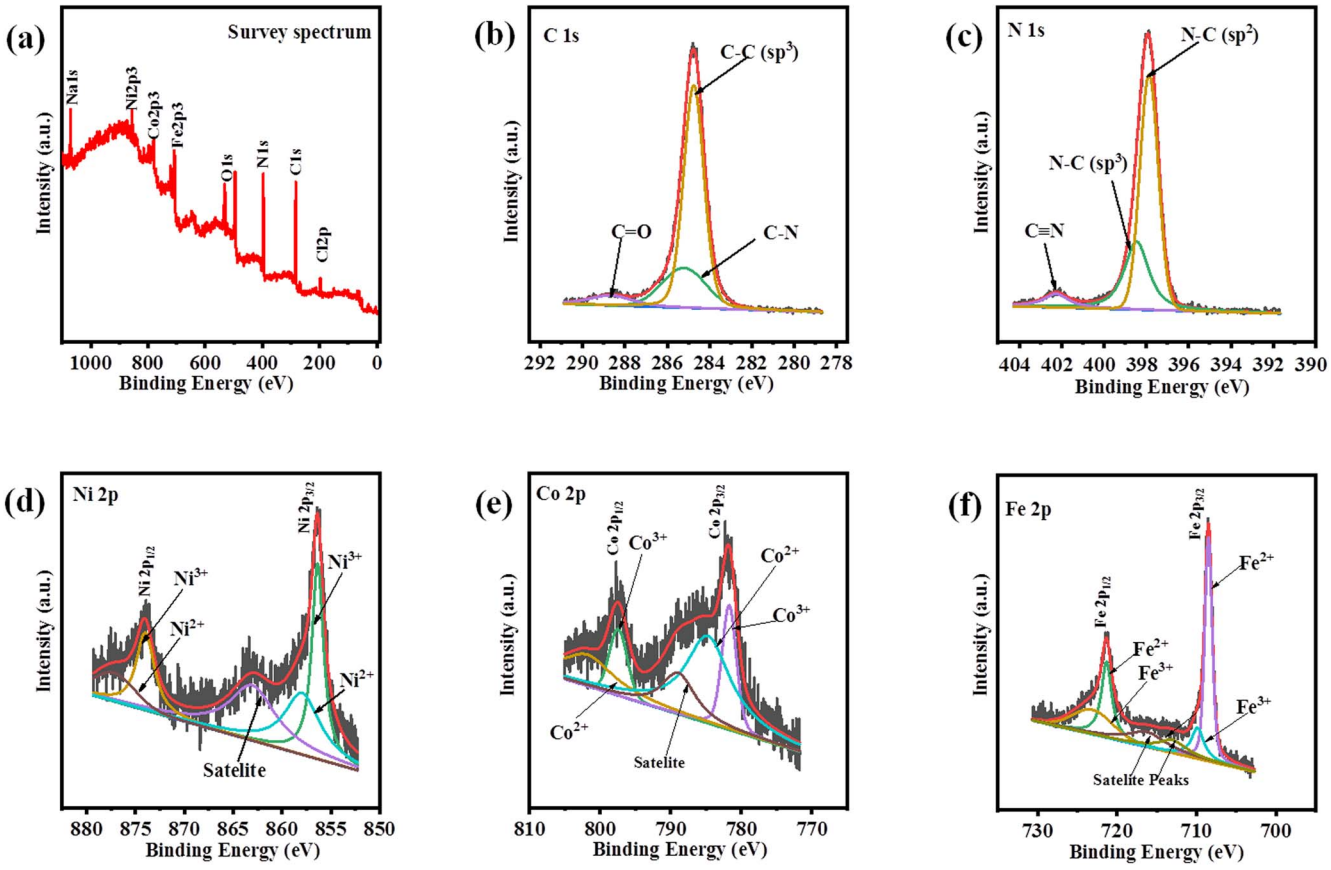

Figure 3. XPS Spectra of pristine $Na_2Ni_{0.33}Co_{0.33}[Fe(CN)_6]$ nanoparticles; Survey spectra (a), XPS spectra of Carbon (b), Nitrogen (c), Nickel (d), Cobalt (e) and Iron (f).

second with the same scale, confirms the sodium has been removed from the sample while charging and reinserted while discharging. The Figs. 5b and 5f shows the Ni 2*p* peaks centered at 855.33 eV and 857.38 eV corresponds to Ni $2p_{3/2}$ Ni^{3+} and Ni^{2+} states respectively, whereas the peaks centered at 873.49 eV and 876.19 eV corresponds to Ni $2p_{1/3}$ Ni^{3+} and Ni^{2+}. The additional peaks centered at 859.49, 862.73 and 880.65 eV are satellite peaks. The intensity and the binding energy corresponds of Ni in discharged state shows slight variation compared to that of charged state, indicating that it can have slight influence in the voltage window.[29,30] Figures 5c and 5g shows the Co 2*p* peaks centered at 781.18 eV and 784.12 eV corresponds to Co $2p_{3/2}$ Co^{3+} and Co^{2+} respectively, whereas the peaks centered at 797.15 eV and 802.43 eV corresponds to Co $2p_{1/3}$ Co^{3+} and Co^{2+} respectively. The peak at 788.27 corresponds to satellite peak. The oxidation peaks of Co at charged and discharged state also has slight variation in the binding energy, indicating that Co can influence the voltage window slightly.[31] Figures 5d and 5h shows the Fe 2*p* peaks centered at 708 eV and 709.23 eV corresponds to Fe $2p_{3/2}$ Fe^{3+} and Fe^{2+} states respectively, whereas the peaks centered at 720.94 eV and 725.39 eV corresponds to Fe $2p_{1/3}$ corresponding to Fe^{3+} and Fe^{2+} respectively.[32,33] For Fe, there are two satellite peaks observed at 715.67 and 712.31 eV. The intensity of Fe peak corresponding to the discharged state shows high variation in the binding energy while comparing with charged state. The intensity of Fe^{3+} and Fe^{2+} peaks are almost equal at discharged state and Fe^{2+} peak intensity is much higher than that of Fe^{3+} state in charged state, suggesting that the Fe^{3+}/Fe^{2+} redox occurs during the sodiation/desodiation process. The XPS analysis after the

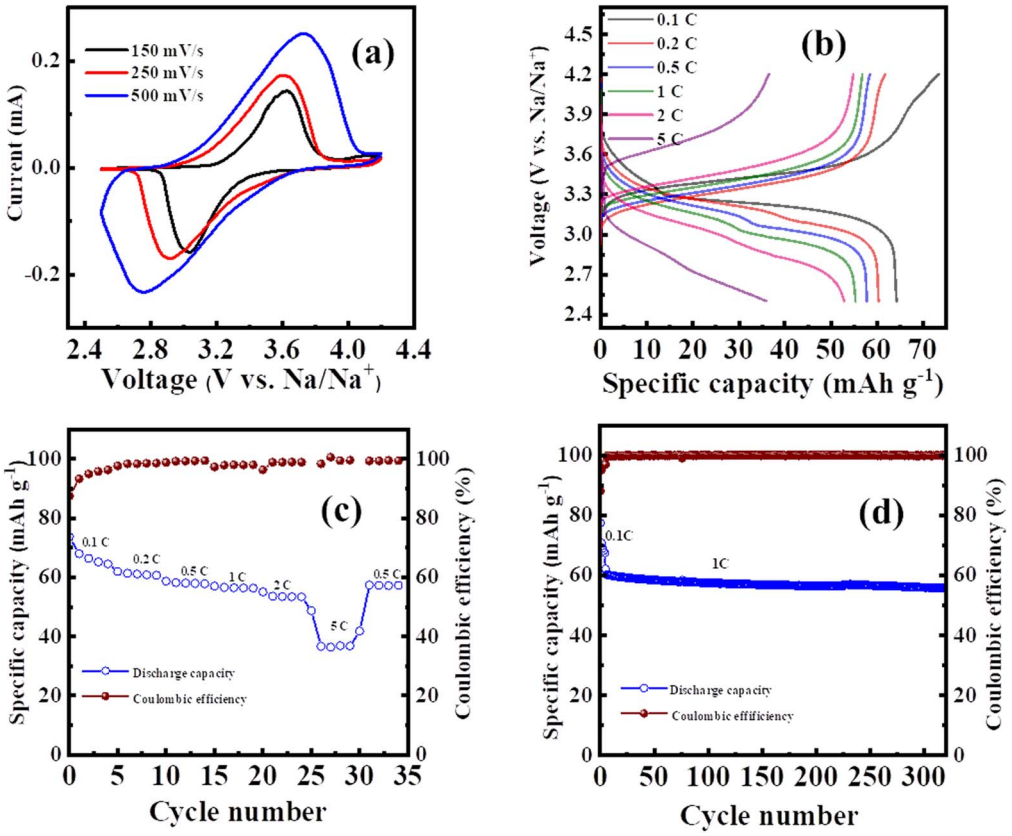

Figure 4. Electrochemical performance of $Na_2Ni_{0.33}Co_{0.33}[Fe(CN)_6]$ cathode for Na-ion batteries. (a) Cyclic voltammogram of $Na_2Ni_{0.33}Co_{0.33}[Fe(CN)_6]$ cathode at different scan rate. (b) Charge-discharge voltage profile of $Na_2Ni_{0.33}Co_{0.33}[Fe(CN)_6]$ cathode at different C rate. (c) Charge and discharge capacity and Columbic efficiency of $Na_2Ni_{0.33}Co_{0.33}[Fe(CN)_6]$ cathode at different C rates. (d) Charge capacity and Columbic efficiency of $Na_2Ni_{0.33}Co_{0.33}[Fe(CN)_6]$ nanoparticles at 1C rate upto 310 cycles.

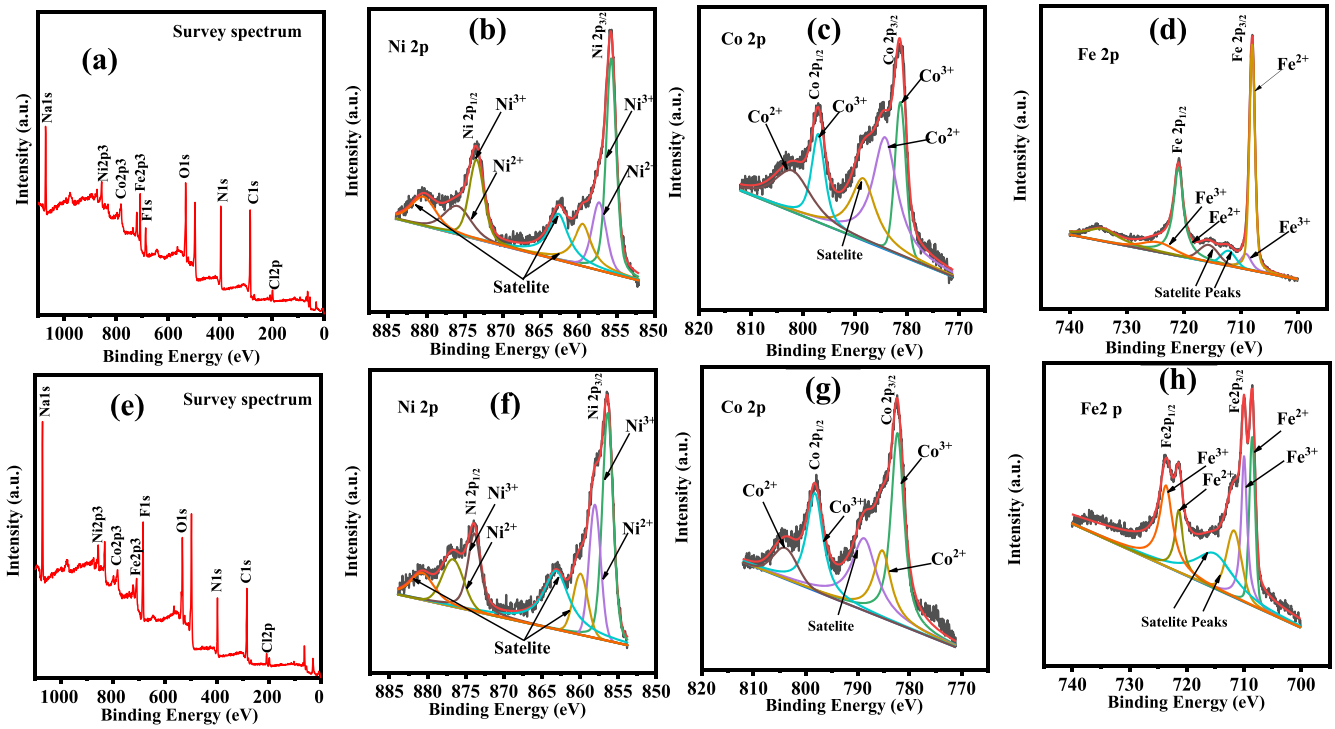

Figure 5. Ex situ XPS spectra of $Na_2Ni_{0.33}Co_{0.33}[Fe(CN)_6]$ electrodes after the 1st charge (a) to (d) and 2nd discharge (e) to (h).

Table I. Electrochemical properties of few PB materials reported in the literature.

S.No	Material	Voltage (V)	Discharge Capacity (mAh/g)	Cycles/C-Rate	References
1	$Na_2Ni[Fe(CN)_6]$	3.2	71	450/1C	1
2	$Na_{1.67}Ni[Fe(CN)_6]_{0.87}$	3.2	42	1200/170 mAg^{-1}	2
3	$Na_2Co_3[Fe(CN)_6]_2$	3.2	36	50/200 mAg^{-1}	3
4	$Cu_3[Fe(CN)_6]_2$	3.2	15	100/20 mAg^{-1}	4
5	$Na_{0.84}Ni[Fe(CN)_6]_{0.71}$	3	65	200/ 20 mAg^{-1}	5
6	$Na_2Ni_{0.33}Co_{0.33}[Fe(CN)_6]$	3.2	55	320/1C	This work

electrochemical reaction clearly indicates that the Fe^{3+}/Fe^{2+} redox happened predominantly in the $Na_2Ni_{0.33}Co_{0.33}[Fe(CN)_6]$ structure during the electrochemical reaction.

Conclusions

The $Na_2Ni_{0.33}Co_{0.33}[Fe(CN)_6]$ nanoparticles were synthesized by facile and low temperature synthesis method. The $Na_2Ni_{0.33}Co_{0.33}[Fe(CN)_6]$ Prussian blue analogous exhibits oxidation peak at 3.5 V and reduction peak at 3 V, which is favorable for the possibility of fabricating non-aqueous Na-ion battery. The $Na_2Ni_{0.33}Co_{0.33}[Fe(CN)_6]$ nanomaterials has delivered a charging capacity of 77 mAh g^{-1} at the first cycle with 0.1C rate. The charge capacity is seen to be 62 mAh g^{-1} at the first cycle and 55 mAh g^{-1} after 320th cycle at 1C rate. Coulombic efficiency is seen to be 100% throughout the charge/discharge cycle at different C rates. The XPS analysis after the electrochemical reaction indicates that the Fe^{3+}/Fe^{2+} redox is predominant in the $Na_2Ni_{0.33}Co_{0.33}[Fe(CN)_6]$ structure during the electrochemical reaction.

ORCID

Akhil Shettigar https://orcid.org/0000-0001-9529-4686
K. Kamala Bharathi https://orcid.org/0000-0002-8466-9400

References

1. W. Ren, X. Chen, and C. Zhao, *Adv. Energy Mater.*, **8**, 1801413 (2018).
2. E. A. Olivetti, G. Ceder, G. G. Gaustad, and X. Fu, *Joule*, **1**, 229 (2017).
3. T. Wang, D. Su, D. Shanmukaraj, T. Rojo, M. Armand, and G. Wang, *Electrochem. Energ. Rev.*, **1**, 200 (2018).
4. Y. Huang, Y. Zheng, X. Li, F. Adams, W. Luo, Y. Huang, and L. Hu, *ACS Energy Lett.*, **3**, 1604 (2018).
5. J.-Y. Hwang, S.-T. Myung, and Y.-K. Sun, *Chem. Soc. Rev.*, **46**, 3529 (2017).
6. B. L. Ellis, W. R. M. Makahnouk, Y. Makimura, K. Toghill, and L. F. Nazar, *Nat. Mater.*, **6**, 749 (2007).
7. P. Barpanda, G. Oyama, S. Nishimura, S.-C. Chung, and A. Yamada, *Nat. Commun.*, **5**, 4358 (2014).
8. Y.-U. Park, D.-H. Seo, H. Kim, J. Kim, S. Lee, B. Kim, and K. Kang, *Adv. Funct. Mater.*, **24**, 4603 (2014).
9. N. Yabuuchi, M. Kajiyama, J. Iwatate, H. Nishikawa, S. Hitomi, R. Okuyama, R. Usui, Y. Yamada, and S. Komaba, *Nat. Mater.*, **11**, 512 (2012).
10. E. Talaie, V. Duffort, H. L. Smith, B. Fultz, and L. F. Nazar, *Energy Environ. Sci.*, **8**, 2512 (2015).
11. S. Mariyappan, Q. Wang, and J. M. Tarascon, *J. Electrochem. Soc.*, **165**, A3714 (2018).
12. J. Peng et al., *Adv. Energy Mater.*, **8**, 1702856 (2018).
13. Y. Xu et al., *Adv. Energy Mater.*, **9**, 1803158 (2019).
14. A. Bauer, J. Song, S. Vail, W. Pan, J. Barker, and Y. Lu, *Adv. Energy Mater.*, **8**, 1702869 (2018).
15. L. Shen, Z. Wang, and L. Chen, *Chemistry—A European Journal*, **20**, 12559 (2014).
16. W. Gong, M. Wan, R. Zeng, Z. Rao, S. Su, L. Xue, W. Zhang, and Y. Huang, *Energy Technology*, **7**, 1900108 (2019).
17. Y. Lu, L. Wang, J. Cheng, and J. B. Goodenough, *Chem. Commun.*, **48**, 6544 (2012).
18. C. D. Wessells, R. A. Huggins, and Y. Cui, *Nat. Commun.*, **2**, 550 (2011).
19. Y. You, X. Yu, Y. Yin, K.-W. Nam, and Y.-G. Guo, *Nano Res.*, **8**, 117 (2015).
20. D. S. Kim, M. B. Zakaria, M.-S. Park, A. Alowasheeir, S. M. Alshehri, Y. Yamauchi, and H. Kim, *Electrochim. Acta*, **240**, 300 (2017).
21. X. Wu, C. Wu, C. Wei, L. Hu, J. Qian, Y. Cao, X. Ai, J. Wang, and H. Yang, *ACS Appl. Mater. Interfaces*, **8**, 5393 (2016).
22. M. Takachi, T. Matsuda, and Y. Moritomo, *Appl. Phys. Express*, **6**, 025802 (2013).
23. L. Wang, Y. Lu, J. Liu, M. Xu, J. Cheng, D. Zhang, and J. B. Goodenough, *Angew. Chem. Int. Ed.*, **52**, 1964 (2013).
24. L. Wang et al., *J. Am. Chem. Soc.*, **137**, 2548 (2015).
25. M. Takachi, T. Matsuda, and Y. Moritomo, *Jpn. J. Appl. Phys.*, **52**, 090202 (2013).
26. X. Wu, Y. Cao, X. Ai, J. Qian, and H. Yang, *Electrochem. Commun.*, **31**, 145 (2013).
27. J. Qian, C. Wu, Y. Cao, Z. Ma, Y. Huang, X. Ai, and H. Yang, *Adv. Energy Mater.*, **8**, 1702619 (2018).
28. W. Li, F. Zhang, X. Xiang, and X. Zhang, *J. Phys. Chem. C*, **121**, 27805 (2017).
29. Y. Shen et al., *Nanoscale*, **11**, 11765 (2019).
30. Y. Feng, X.-Y. Yu, and U. Paik, *Chem. Commun.*, **52**, 6269 (2016).
31. H. Fang et al., *J. Mater. Chem. A*, **7**, 7328 (2019).
32. W. Qi, S. Liu, F. Li, H. Jiang, Z. Cheng, S. Zhao, and M. Yang, *Catal. Sci. Technol.*, **9**, 2571 (2019).
33. P. Xiong, G. Zeng, L. Zeng, and M. Wei, *Dalton Trans.*, **44**, 16746 (2015).
34. K.-Y. A. Lin and B.-J. Chen, *J. Colloid Interface Sci.*, **486**, 255 (2017).
35. K. Siuzdak, M. Szkoda, J. Karczewski, J. Ryl, and A. Lisowska-Oleksiak, *RSC Adv.*, **6**, 76246 (2016).
36. R. Thangavel, M. Moorthy, B. K. Ganesan, W. Lee, W.-S. Yoon, and Y.-S. Lee, *Small.*, **16**, 2003688 (2020).
37. R. Thangavel, A. G. Kannan, R. Ponraj, G. Yoon, V. Aravindan, D.-W. Kim, K. Kang, W.-S. Yoon, and Y.-S. Lee, *Energy Storage Mater.*, **25**, 702 (2020).